

# TIME-EFFICIENT H-MAPPING TECHNIQUE EMBEDDED IN BUILDING ENERGY MODELS

*L. Hach*<sup>1</sup>, *K. Hemzal*<sup>2</sup>

1Yamaguchi University, Collaborative Research Center,  
Tokiwadai 2-16-1, Ube 755-8611, Japan,

2 Faculty of Mechanical Engineering CTU Prague, Technicka 4, 166 07 Prague, Czech Rep.

## Abstract

**Object identification and indoor airflow simulation are utilized in this work in order to provide an effective tool in energy performance evaluation of an occupied space in the residential building [2], [3]. Principal calculation of heat exchange through the space envelope includes heat flow rate in terms of heat transfer (U-value) coefficients. An accurate and time-effective way of obtaining them through MATLAB procedure is presented here.**

## 1 Thermal Object Modelled in MATLAB Environment

A single-zone model was assembled in order to predict thermal behavior of a space within the residential building located in the mild climate zone on southern part of Honshu Island (Japan) [1]. It consists of three inner walls, two of them symmetrically neighboring similar rooms, each of them on opposite sides, while the remaining outside wall is south-west oriented and 50%-glassed, Fig. 1.

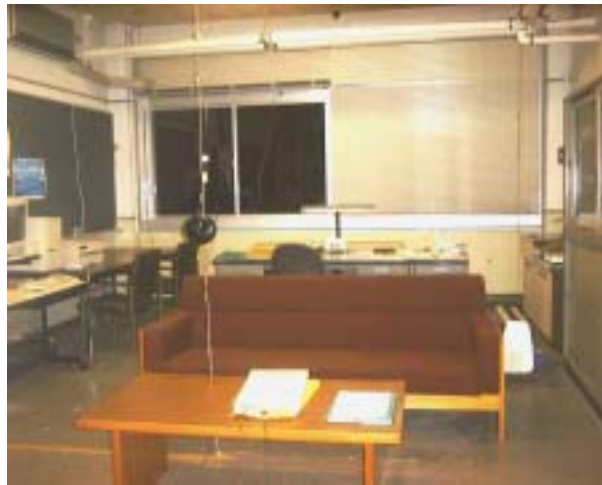


Figure 1: Insight view of reference room with installed globe (Vernon) thermometer in the interior's center

The administrative building's light type reinforced concrete structure of the building with insufficient  $U$ -value ( $U \cong 3,1$ ) supplied by steam central heating system (CHS) in winter heating period makes inner spaces vulnerable to outside climate changes in terms of inadequate thermal constants of outer wall-ceiling's thermal mass-CHS control adaptability. The energy balance of the space is influenced by interaction with the environment via radiation, heat conduction and convection; of these three phenomena convection, and in particular infiltration, influences the overall air flow regime, which in turn affects adjacent layers crucial for actual convective heat transfer occurring on the most cold (winter conditions) outdoor wall.

Our case is based on quasi-equilibrium energy balance equation (in specific heat amount per time unit):

$$dQ_h(\tau) = dQ_t(\tau) + dQ_v(\tau) + dQ_{vc}(\tau) - \sum_j dQ_{i_j}(\tau) - dQ_{s,wo}(\tau) - dQ_{s,wf}(\tau) \quad (\text{J}\cdot\text{s}^{-1}) \quad (1)$$

- where:
- $Q_h$  - heat rate covered by heater (W)
  - $Q_i$  - heat rate of internal heat sources (W)
  - $Q_h$  - heat amount excerpt of occupant (internal heat source: human body) (W)
  - $Q_{s,wf}$  - transmitted solar radiation heat rate through window (W)
  - $Q_{s,wo}$  - transmitted solar radiation heat rate through exterior wall (W)
  - $Q_t$  - heat rate through wall (heat conduction) (W)
  - $Q_v$  - heat rate by infiltration (W)
  - $Q_{vc}$  - heat rate by controlled ventilation (W)
  - $j$  - number of internal heat sources.

The energy flows in Eq. (1) through the observed space ( $L \times B \times H$ : 7250 x 4550 x 3000 mm) and thus for the model development, basic relations of physical phenomena that govern the thermal energy transfer process, were employed [1]. The model block structure in Simulink tool environment shows Fig. 2:

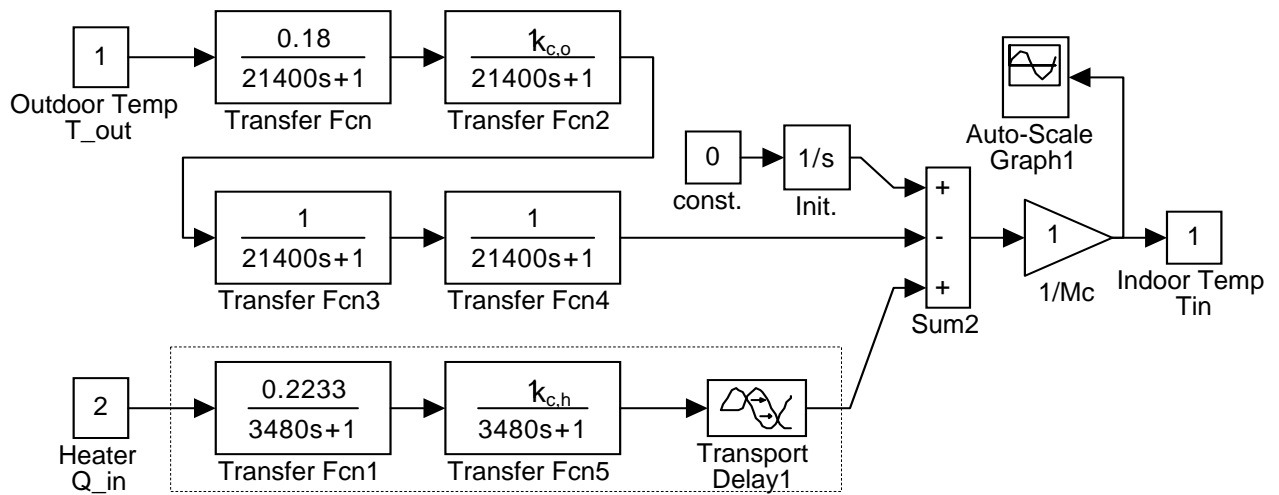


Figure 2: Reference room module with steam heater transient function (transfer blocks  $Fcn1$ ,  $Fcn5$  and transport block  $Delay 1$ )

The simulated indoor temperature  $T_{in}$  in Fig. 2 was product of internal heat sources (i.e. heater and other heat producing devices, occupants) and outdoor climate influences (outdoor air temperature, wind, sun radiation).

## 2 Heat Transfer on Vertical Outdoor Wall

### 2.1 6-Nodal Model of 1-Dimensional Conduction

The contribution to the inside air  $T_a$ , and therefore, to the global indoor temperature from convective heat transfer along the outdoor vertical wall were investigated. At first, the one-dimensional heat transfer, occurring through the wall, was calculated in a conventional way and the iterative calculation of Fourier formula [1], [6] was embedded onto the MATLAB procedure, Fig. 3:

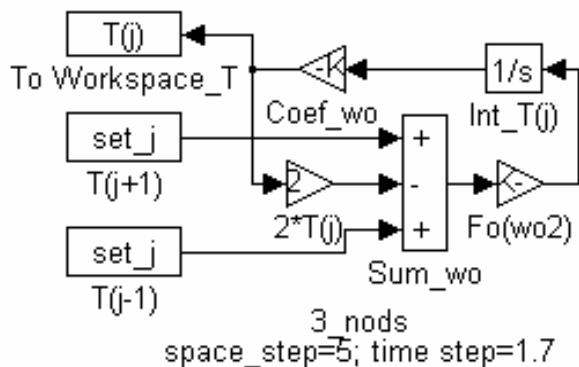


Figure 3: Basic thermal analog of temperature mapping within isotropic slab.  $T(j-1)$ ,  $T(j)$ ,  $T(j+1)$  – temperatures of spatial line-up in one – dimensional heat flow data set,  $Int\_T(j)$  – integr. with initial temperature value,  $Coef\_wo$ ,  $Fo(wo2)$ ,  $2*T(j)$  – multipliers

Each wall was subjected to the above described procedure and the values of the temperature gradients were determined through a simple computational model, as is shown in the Fig. 4, used on the outside wall (6 nodes, accuracy  $\pm 10\%$ ):

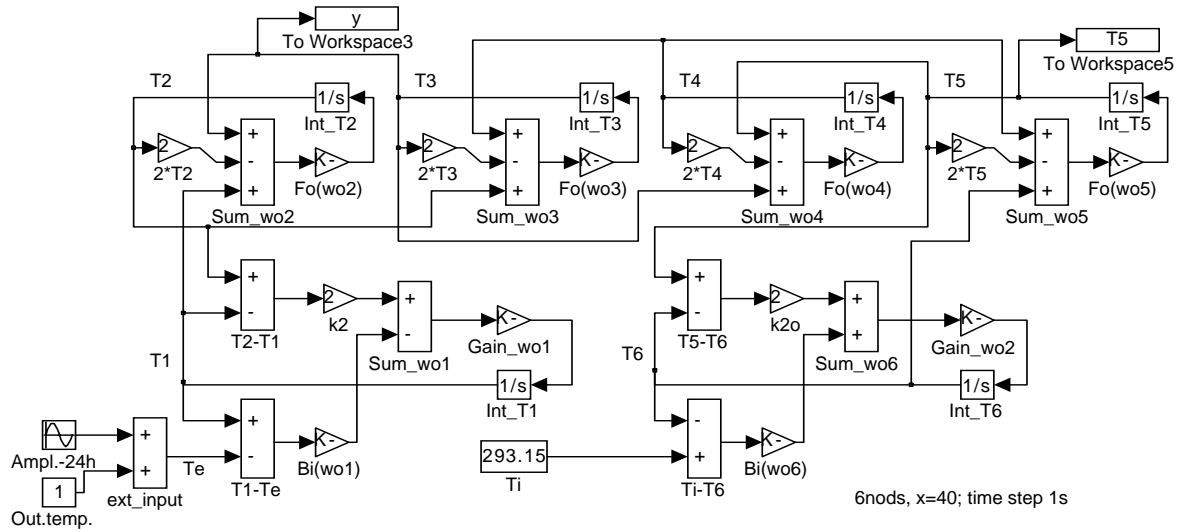


Figure 4: Analog of outside wall temperature distribution with convective boundary conditions

Surface and nodal temperatures within the  $k$ -wall were linked through relation ( $j$  – number of nodes):

$$T_{w,i,k}(\tau) = f[T_{w_j}(x, \tau)], \quad j = 1, 2, \dots, 7 \quad (\text{K}) \quad (2)$$

and evaluation of the damping of harmonic change of ambient temperature  $\nu$  in the indoor air, Eq. (3), indicated poor thermal insulation on surrounding walls – over 0,23:

$$\nu = \frac{\Delta t_i}{\Delta t_e} = \left[ 1 + \sqrt{2} \frac{s}{h_e} + \left( \frac{s}{h_e} \right)^2 \right]^{\frac{1}{2}} \cdot e^{-\frac{R_s}{\sqrt{2}}} \cdot \left[ 1 + \sqrt{2} \frac{h_i}{s} + \left( \frac{h_i}{s} \right)^2 \right]^{\frac{1}{2}} \quad (-) \quad (3)$$

- where
- $\Delta t_i$  2 amplitudes of wave of indoor temperature (K)
  - $\Delta t_e$  2 amplitudes of wave of ambient air (K)
  - $h_e, h_i$  heat transfer coefficient of outdoor (inside) faced outside wall ( $\text{Wm}^{-2} \text{K}^{-1}$ )
  - $R$  wall thermal resistance ( $\text{m}^2 \text{K W}^{-1}$ )
  - $s$  thermal absorption while harmonic temperature change,  $s = (2\pi\lambda\rho c / \tau_0)^{1/2}$  ( $\text{Wm}^{-2} \text{K}^{-1}$ )
  - $\tau_0$  time period (24 hours)

## 2.2 $h_{cv}$ - Mapping in MATLAB 3D-Matrix

The tested space disposition with a spatial symmetry along the room's (main) meridian together with thermally equal adjacent spaces (i.e. heated on the same heating regime over a period of time) created boundary conditions favourable to the recirculating airflow regime. The air flow is in some extent symmetrical around the space meridian, where also thermal sensors were placed (in Fig. 1 visible the globe thermometer). Together with sensors ( $T$ -type thermocouples), placed on walls and glass pane surfaces, data was registered on the data logger with simple programme (see Appendix, Basic lang. source code). The code should work on a data acquisition unit with the Basic code (in our case lic. Hewlett-Packard unit). It screened cca 32 channels (thermocouples) in non-stop cycle and recorded them to a predefined storage space onto the personal computer (PC) connected to the serial port RS-232 via data link cable. The measured data allows to calculate the local convective heat

transfer coefficient  $h_{cv}(x)$  from the rate of convective heat transfer  $q_{cv}(x)$  and the temperature difference between the surface and the relevant air temperature [2]:

$$h_{cv}(x) = \frac{q_{cv}(x)}{[T_w - T_a(x)]} \quad (4)$$

The average heat-transfer coefficient in free or forced-convection regime yields the integration of

$$\bar{h}_{cv} = \frac{1}{H} \int_0^H h_{cv}(x) dx \quad (5)$$

where  $H$  denotes wall height (m), with local heat transfer coefficients  $h_{cv}(x)$  obtained from the dimensionless, basic formula:

$$Nu(x) = K [Gr(x) \cdot Pr]^n \quad (6)$$

In a near quasi-steady thermal state, the falling cooled air mass along the cooled inner surface confronted warmer air flow from heater in opposing directions until the two currents reached stand-still at some point above the heater. In this area both air masses partly mix and partly divert themselves around a newly formed *near-still-zone* in its core. The larger the value of the Grashof-Prandtl product in Eq. (6), the better results the free-convection formula yields. Quite comprehensive overview over convective coefficients embedded into building energy models offers [3], some other empirical (semi-empirical) formulas are summarized in [4], Chap. 7.

The resulting flow pattern inside the enclosure was solved by the Navier–Stokes equation (NS) with dimensionless governing equations of continuity, momentum and energy equations in steady-state form in meridian cut:

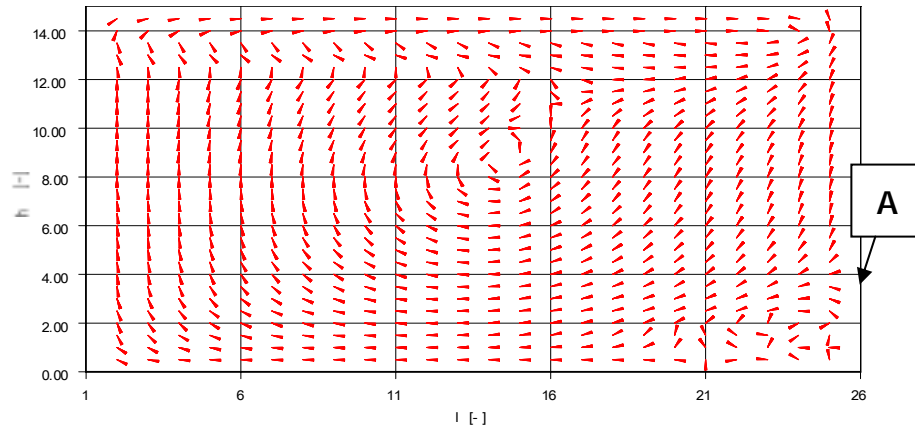


Figure 5: 2D-velocity field of air movement at the meridian plane of non-uniformly cooled space; Air change ratio 0.5

In case of same stable core (not rolling upwards/downwards), see the arrow  $A$  in Fig. 5, adjacent layers divert away from the core and still bear the convective part, while slowly moving core  $A$  will contribute rather with the conductive portion of  $\frac{s_y}{\lambda_a}$ , where  $s_y$  (m) is the characteristic dimension of the core in perpendicular direction to the wall and  $\lambda_a$  ( $\text{W}\cdot\text{m}^{-1}\cdot\text{K}^{-1}$ ) air conductivity. The conductive part was superposed on the standard coefficient  $h_{cv}$ , Eq. (5), on the same enclosure meridian where 2D-velocity and temperature patterns mirror themselves at best, compared to the other planes parallel with the meridian. The MATLAB-written portion of the formula  $h_{cv} = h_{cv}(T_a - T_{wo}; H)$  with plot output is included in Appendix. In Fig. 6 it is compared with two  $h_{cv}$ -algorithms according to Hollman [4] and Alamdari and Hammond [5]:

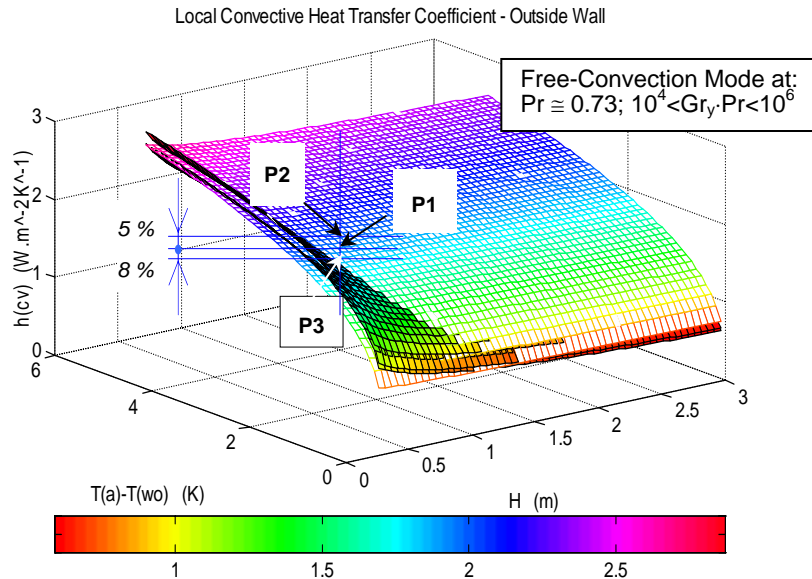


Figure 6: Convective heat transfer coefficient of isothermally cooled vertical wall,  $h_{cv} = f(H, T_a - T_w)$ . Comparison for [1.1 m; 3 K]: P1 – this study, P2-Alamdari & Hammond [5] (difference 8%), P3 – Holman [4] (difference 5%)

The  $h_{cv}$ -differences yielded from Fig. 6 on rather higher (vertical) distances and widened surface-air temperature gaps; however, already for  $H = 1.1$  m and  $T_a - T_w \cong 2$  K, i.e. point P2 in Fig. 6 (Alamdari and Hammond [5]), indicates an 8 %-increase in a quite wide Grashof - Prandtl product range of  $10^4 < Gr \cdot Pr < 10^6$ ,  $Pr \cong 0.73$ .

### 3 Results

The  $h_{cv}$ -comparisons with and without the near-stand-still zone on the vertical wall on the same meridian are plotted in Figures 7 and 8 over an actual height of 2.85 m and the surface-air temperature differences up to 5 K.

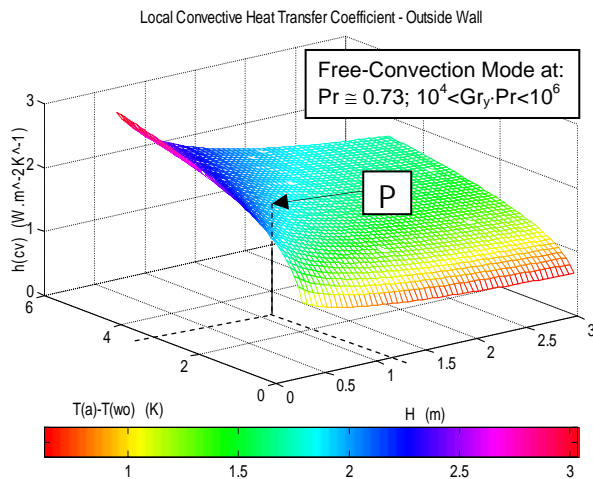


Figure 7:  $h_{cv}$ -surface graph of vertical wall with non-still-air area  $h_{cv} = f(H, T_a - T_{w0})$ ,  $ACH = 0.5$ . At point P = [1.1m; 3K]:  $h_{cv} = 1.93 \text{ W.m}^{-2} \cdot \text{K}^{-1}$

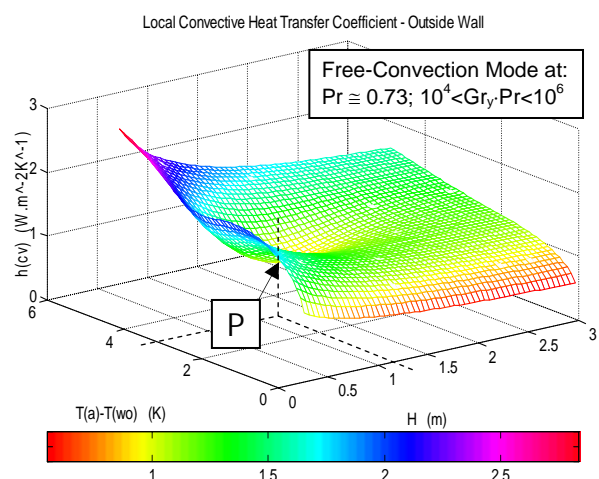


Figure 8:  $h_{cv}$  - surface graph of vertical wall with developed still-air area  $h_{cv} = f(H, T_a - T_{w0})$ ,  $ACH = 0.5$ ,  $\Delta T_a = (295.5 \div 297.3) \text{ K}$

The convective surface plane in Fig. 7 is extracted  $h_{cv}$ -surface plane from Fig. 6 (Alamdari & Hammond) i.e. the original, non-still-air-zone. It would 'become flatter' as expected on the wall strip

area beneath the stagnation zone (point *A* at Fig. 5) from the moment being formed. There are  $h_{cv}$ -planes superposed from two semi-empirical  $h_{cv}$ -algorithms of the local Nusselt number  $Nu_x = K \cdot Ra_x^n$  (Eq. (6)) for opposite flows in the Fig. 8:

$$h_{cv}(x) = 1.5 \left[ \frac{T_w - T_a(x)}{x} \right]^{1/4} - \frac{1}{a + (x - x_{sz})^2} - \frac{1}{b \{ [T_w - T_a(x)] - (T_w - T_a)_{sz} \}^2} \quad (7)$$

for an otherwise unchanged *ACH*-value (air change ratio) and surface wall temperature gradient  $-k_w \left[ \frac{\partial T_w}{\partial y} \right]_{y=0}$ . Although the correlation in Eq. (7) is subject to restrictions over the temperature and

dimension ranges of the free-convection mode on a vertical wall, it is applicable for:

- $x_{sz}$  – stagnation zone height (m) around the half of wall height, and
- $(T_w - T_a)_{sz}$  surface-air temperature difference at the stagnation zone height (m)
- $a, b$  – coefficients depending on aspect ratio  $a_r$  of the stagnation zone (-);  $a = 1.0$ ;  $b = 1$
- $a_r$  – ratio = surface-air temperature distance/stagnation zone characteristic dimension).

The  $h_{cv}$ -value change was estimated in a thermal state of the wall-air temperature difference of 3 Kelvins at 1.1 meters above floor (point *P* = [3 K; 1.1 m]). It amounted to about 48 % decrease as result of higher heater output in Fig. 8, corresponding to weaker buoyancy forces. The higher heater output boosted the surface-air temperature difference with the upward air stream, therefore curbing further the lower part of  $h_{cv}$ -map as is shown in Fig. 8, while the weaker buoyancy force upwards corresponds to lesser  $h_{cv}$ -decrease than indicated on Fig. 8.

The pre-defined set of  $h_{cv}$ -maps do not require the MATLAB application running all the time with sufficient storage capacity of 3D-MATLAB matrices in an outside-MATLAB-recognizable format (for inst. Excel-format).

## Appendix

### PROGRAM 'KISHOU 6' (BASIC N 88)

```

10 REM "PROGRAM READ&RECORD CLIMATE DATA 'KISSHOU'"
60 REM
80 SAVE "kishou6.bas",A
90 REM
100 SC=11
110 ISET IFC
120 ISET REN
123 REM
130 CMD TIMEOUT=0
133 REM
140 CMD DELIM=0
143 REM
150 POLL SC, STB
160 ON SRQ GOSUB *SRQI
163 REM AUTO 10
170 '
180 OPEN "B:DATD2-22.DAT" FOR OUTPUT AS #1
200 PRINT@ SC;"*CLS"
210 PRINT@ SC;":CH7:TEMP T"
220 PRINT@ SC;":COPY CH7,CH8,CH31"
230 PRINT@ SC;":SCAN:INTERVAL 0,0,150"
240 PRINT@ SC;":SCAN:CH 7,31"
250 PRINT@ SC;":HEADER ON"
260 PRINT@ SC;":TRIG:COMM REPEAT"
270 PRINT@ SC;"*SRE 1"
280 REM

```

```

300 *LOOP:
310 SRQF=0
320 PRINT@ SC;"*TRG"
330 '
340 SRQ ON
350 IF SRQF=0 GOTO 350
360 TRG=STB AND 1
370 IF TRG <> 1 THEN SRQF = 0 : GOTO 340
380 '
390 PRINT@ SC;":TRGR?" : INPUT@ SC;D$
400 REM
410 REM
420 REM SC
430 PRINT@ SC;":READ:SCAN:TIME?"
440 INPUT@ SC;T$ :PRINT " TIME ";T$
450 WRITE #1,T$
460 FOR CH=7 TO 31
470 PRINT@ SC;":READ:CH"+RIGHT$(STR$(CH),LEN(STR$(CH))-1)+"?"
480 INPUT@ SC;D$ : PRINT D$
485 WRITE #1, D$
490 NEXT CH
500 REM CLOSE #1
510 PRINT : GOTO *LOOP
520 '
530 REM
540 *SRQI
550 SRQF=1
560 REM CONT
570 POLL SC,STB
580 RETURN
590 CLOSE #1
610 END

```

*Measurement data control program (Standard Basic N88).*

### **MATLAB Subroutine for $h_{cv}$ -Maps Plotting**

```

% Axis x: height H=3 m
x=0.3:0.05:3;
% Axis y: T(air)-T(wall)
y=0.1:0.1:4.9;
[x_grid,y_grid]=meshgrid(x,y);

% graph superposition
z1=1./(x_grid);
z2=y_grid.*z1;
z3=1.5*(z2.^0.25);
z4=1./(1.+(x_grid-1).^2+(y_grid-3).^2)
z=z3-z4;

surf(x_grid,y_grid,z);
grid on
title('Local Convective Heat Transfer Coefficient - Outside Wall'),...
    ylabel('T(a)-T(wo) (K)'),zlabel('h(cv) (W.m^-2K^-1)'),...
    xlabel('H (m)');

colorbar('horiz')
axis ([0 3 0 6 0 3])
end

```

## References

- [1] Hach, L., Katoh, Y. *Application of Quasi-Steady-State Thermodynamic Model of Conventional Heating System with Takahashi Control Method*. The 7th International Conference of Building Simulation BS2001, Proceedings. Rio de Janeiro, August 2001.  
[http://www.hvac.okstate.edu/pdfs/bs01/BS01\\_0889\\_896.pdf](http://www.hvac.okstate.edu/pdfs/bs01/BS01_0889_896.pdf)
- [2] Merkin, J.H. *Natural-convection boundary-layer flow on vertical surface with Newtonian heating*. Int. Journal Heat and Fluid Flow 15: 392-398, 1994.
- [3] Beausoleil-Morrison, I. *The Adaptive Simulation of Convective Heat Transfer at Internal Building Surfaces*, Building and Environment 37 (8-9) 791-806, 2002.
- [4] Holman, J., P. *Heat Transfer*, 7th edition in SI units, McGraw-Hill Book Co., pp. 331-362, 1992.
- [5] Alamdari, F. and Hammond, G.P. *Improved Data Correlations for Buoyancy-Driven Convection in Rooms*, Building Services Engineering Research and Technology, 4 (3) 106-112, 1983.
- [6] Gass, J., Hach L., Hemzal, K. *Application of Quasi-Steady-State Thermodynamic Model of Large Low-Temperature Radiant Heating System with TCM*; Proceedings of The 1st International Conference on Heat Transfer, Fluid Mechanics and Thermodynamics (HEFAT), Kruger Park, South Africa, ISBN 0-86970-536-9, Vol.1, Part 1, pp.325-330, April 2002.

---

### Contact information:

Dr.Eng. Lubos Hach, Ph.D.  
Faculty of Chemical Technology  
Pardubice University, Czech Republic  
Tel + 420 (046) 603 6081  
Fax + 420 (046) 603 6033  
Email [lubos.hach@upce.cz](mailto:lubos.hach@upce.cz)